Lasing from conjugated-polymer microcavities

N. Tessler, G. J. Denton & R. H. Friend

Cavendish Laboratory, Madingley Road, Cambridge CB3 0HE, UK

FOLLOWING the discovery[1] of electroluminescence in poly(*p*-phenylenevinylene) (PPV), considerable effort has been directed towards the realization of optoelectronic devices based on semiconducting conjugated polymers of this type[2–6]. But the viability of these materials for such applications depends critically on the nature of the photoexcited states—in particular, whether they are predominantly non-emitting interchain species[7–9] or emitting intrachain species[10]. One way to study this fundamental issue is in a device structure known as a microcavity[11], which offers the possibility of using quantum electrodynamic effects to alter (and hence probe the nature of) spontaneous and stimulated emission in these materials[12–17]. Here we make use of such a structure to demonstrate optically driven laser activity in devices based on solid films of PPV. This demonstration of lasing provides direct support for a model[10] in which the main photoexcitation in PPV is an emissive intrachain species, and opens the possibility of electrically driven polymer-based lasers.

In order to achieve lasing it is advantageous to use a cavity with high quality factor Q, and dimension of the order of the wavelength of the light emitted. The active material in our devices is a film of the polymer PPV (Fig. 1). We chose PPV as it is relatively robust, can show a high photoluminescence efficiency[18] and, in spite of indications to the contrary[7,8,19], it can exhibit gain in pump-probe experiments with ultraviolet excitation, as we show later. As the enhancement of radiation by a microcavity is a strong function of Q we fabricated cavities with highly reflecting mirrors. As the bottom mirror we used a commercially available, ~100-nm-thick distributed Bragg reflector (DBR), which is a stack of alternating layers of high and low refractive indices, with better than 99% reflectivity at visible wavelengths (Comar Limited). To cover the entire visible range, the DBR mirror is made of various stacks with different layer thicknesses (chirped DBR), thus longer wavelengths are reflected deeper inside the stack. This type of mirror causes the cavity length to increase in discrete steps as the wavelength is increased. A virtue of this structure is that, despite the fact that the cavity has a dimension of the order of the wavelength, several discrete modes can still be supported. On top of the DBR we spin-coated a layer of the tetrahydrathiophene

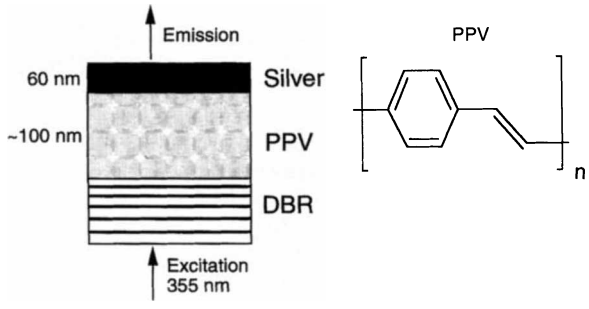

FIG. 1 Structure of the microcavity used. We used different batches of PPV which were converted at various temperatures ($\geq$200 °C) in a vacuum (batch A: bromide, 4 hours conversion; batch B: chloride, 10 hours conversion) to yield PPV films with thicknesses around 100 nm. Depending on the temperature, the films were either substantially or fully conjugated and the solid-state photoluminescence efficiency was measured to be as high as 80% for batch A (using an integrating sphere with 457 nm excitation). The temperature range used in the conversion process had no effect on achieving lasing.

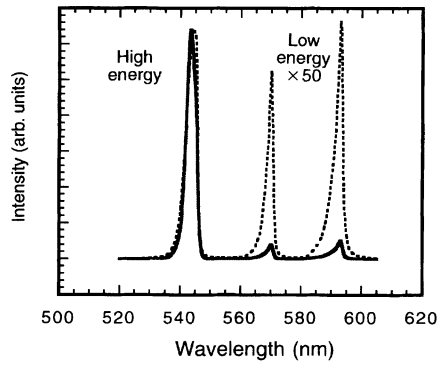

FIG. 2 Emission spectrum of the PPV microcavity structure at two excitation energies, 0.05 μJ and 1.1 μJ. The light was collected from the device, with a 16.5° emission cone (full angle). PPV from batch A was used for this device (see Fig. 1 legend).

halide precursor to PPV[1]. The 60-nm-thick top mirror was formed by the thermal evaporation of silver. Extreme caution was taken to avoid any oxidation of the PPV film[10], and all the above steps were carried out within a dry-nitrogen-filled glovebox. Several devices were made from different batches of PPV.

The devices were excited by the frequency-tripled output of a regeneratively-amplified Nd:YAG laser, consisting of pulses of 200–300 ps, with a repetition rate of 1 kHz and a centre wavelength of 355 nm. The beam was focused to a diameter of 250 μm on the sample and the maximum incident pulse energy was 5 μJ. The sample was excited through the DBR which had 30% transmission at 355 nm. After leaving the sample chamber, the emission was immediately collimated and passed through an adjustable iris which could be set to control the measured emission cone from the device. The photoluminescence spectra were recorded using a spectrograph and a CCD (charge-coupled device) camera.

The measured full width at half maximum (FWHM) of the cavity mode, measured with a 0.8° acceptance cone (full angle), was 1 nm which is close to the 0.65 nm response of the spectrograph, indicating the high Q of the cavity. When the light was collected from a 16.5° cone, the FWHM was ~4 nm. Figure 2 shows the measured photoluminescence spectra for excitation energies (inside the cavity) of 0.05 μJ and 1.1 μJ. At the lower energy, emission is distributed almost equally between three cavity modes that arise from the structure of the DBR mirror. Note that the modes are not equally distributed in energy as their spacing is mainly determined by the wavelength-dependent effective length of the DBR mirror. The dramatic change in the photoluminescence spectrum, with the mode at the PPV gain peak wavelength (545 nm) dominating the emission at high output powers, indicates that the emission is mainly stimulated and hence that the device is lasing. If there were no gain (stimulated emission), the spectrum would just scale with power and no mode would dominate. We also notice that the two additional modes continue to have the same relative power, which is consistent with the presence of gain in the main mode only. These results suggest that by introducing extra modes, the determination of the lasing phenomenon in a wavelength-scale device becomes straightforward.

Figure 3*a* shows the output power of two devices as a function of input power. This figure does not show any abrupt change in the output power (the usual definition of lasing threshold) and this may suggest a high coupling efficiency of spontaneous emission into the lasing mode. In such cases a different criterion for the lasing threshold may be invoked[11]—it is defined as the point at which spontaneous and stimulated emission powers are equal. Figure 3*b* shows the ratio between the integrated power under the lasing mode and the power emitted across the rest of the spectrum. For low powers, where the emission is spontaneous, the ratio for

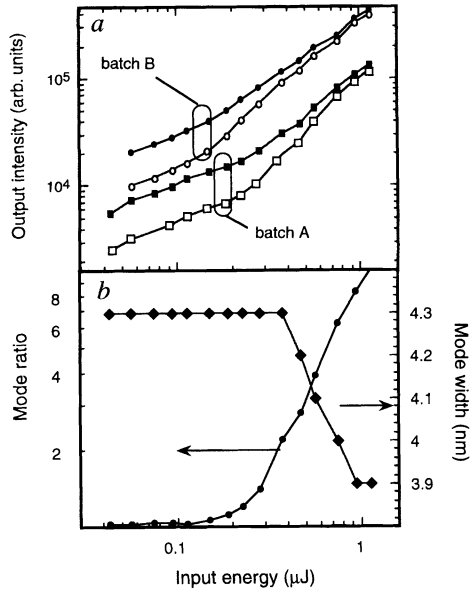

FIG. 3 *a*, Output power as a function of input energy for two microcavity devices made from different PPV batches (Fig. 1 legend). The filled points denote the power integrated between 500 nm and 600 nm and the open points are for the power under the main mode only. *b*, The ratio of the power within the main mode to that in the rest of the spectrum as a function of input energy (filled circles). When this ratio equals two, spontaneous and stimulated emission rates are equal. Also shown is the energy-dependent linewidth of the main mode (filled diamonds). PPV from batch A was used for this device.

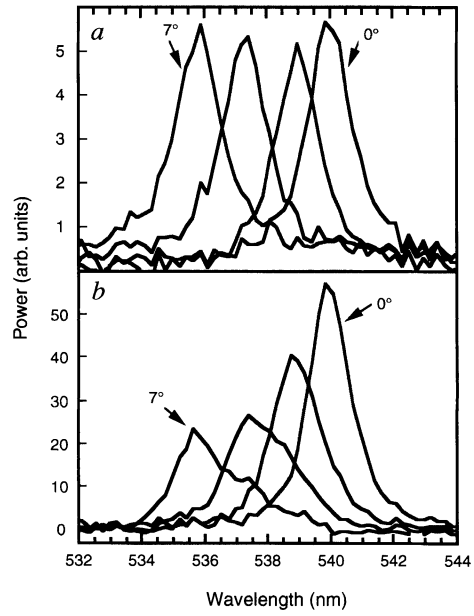

FIG. 4 Output spectra for different viewing angles between 0° (normal direction) and 7°. *a*, Low output power (below lasing threshold). *b*, High output power (above lasing threshold). The increased directionality for high powers is shown by the decrease of peak height with increasing angle. The emission was measured from a 0.8° cone. The curves were shifted horizontally to allow easier comparison between the two subfigures.The measured shift, in the peak wavelength, between the two extreme angles was less than 1 nm.

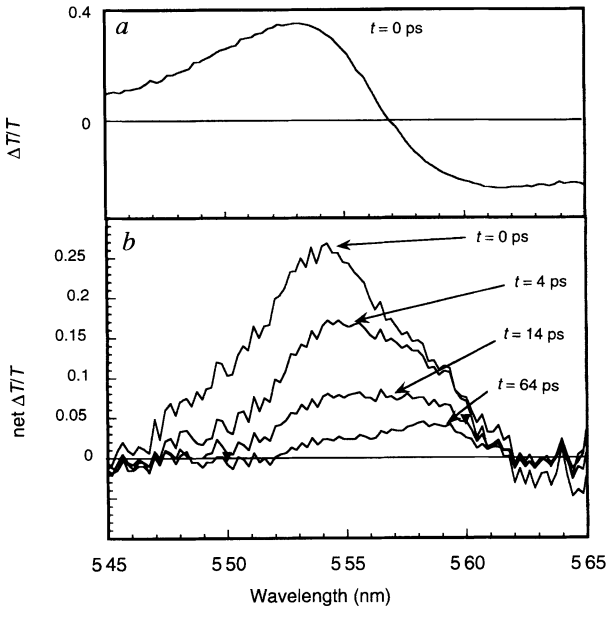

FIG. 5 *a*, Spectrally resolved transient changes in optical transmission, $\Delta T/T$, through a PPV microcavity at delay $t = 0$ after the excitation pulse (at 325 nm). *b*, The same data, shown for a range of delays, after correction for the modulation of the optical cavity length. This gives the net $\Delta T/T$, showing the presence of stimulated emission (gain). The presence of regenerative amplification makes the peak position of the gain follow that of the cavity mode and hence, it also shifts with time. The microcavity was formed with top and bottom silver mirrors (35 nm and 45 nm respectively) sandwiching a ~100 nm film of PPV. The transmission of the device at the resonance wavelength was 2% (the DBR-silver devices had a transmission below the measurement sensitivity). The mode of the cavity was positioned at ~555 nm, close to the PPV peak emission, and had a linewidth of ~10 nm. PPV from batch B was used for this device.

these devices is close to unity. At higher powers, stimulated emission is only present in the lasing mode, and hence this ratio increases. This increase in the relative power within the main mode was also seen in structures that exhibited an additional mode at a shorter wavelength than the main mode. Hence, the ratio change is due to gain in the main mode and not photo-induced absorption which occurs at longer wavelengths[9]. We note that the lasing threshold is reached when this ratio doubles. Also shown in Fig. 3*b* is the power-dependent FWHM of the main mode. Note that the linewidth starts to narrow at the same point, where the mode ratio equals two. The transition from multi-mode to single-mode operation and the narrowing of the linewidth both indicate increased coherence, as expected from a lasing device. Figure 4 shows the angular dependence of the emission spectrum at two output powers (above and below the lasing threshold). The increase in the directionality of emission at high output power (Fig. 4*b*) is further evidence that the device is lasing.

The demonstration of lasing using a solid film of a conjugated polymer also allows us to shed light on a fundamental question related to this type of material. It has been claimed that most of the photoexcited states in this type of polymer are non-emissive interchain polaron pairs and that these are formed instantaneously[7–9]. This non-emissive species was shown to be responsible for photoinduced absorption which masked the gain produced by intrachain excitons[7–9]. If a large number of the interchain species are formed at time $t = 0$, one would not expect lasing even in a microcavity structure. This is both because the microcavity has no effect on the nature of photoexcited states, only on their radiative decay rate, and also because the excited state absorption in the emissive region of the spectrum prevents gain in the cavity.

We find that when the polymer is treated carefully during both synthesis and device preparation, pump-probe measurements at short times after excitation can demonstrate gain, even with ultraviolet excitation. We show this for PPV in a microcavity structure, with silver top and bottom mirrors. These measurements were carried out using the time-resolved differential transmission technique with 150 fs pump pulses at 325 nm (ref. 20). In

this technique, the fractional change ($\Delta T/T$) in the transmission (T) of a broad-band (white-light) probe in the presence of the pump is spectrally resolved and measured as a function of the time delay between the pump and probe pulses. For this cavity structure, effects are due to both the excited state emission and absorption in the PPV, and the modulation of the cavity length as a result of the excited state population (described by the resonant third-order nonlinear optical susceptibility). The latter is evidently a response that follows the differential of the cavity mode function with respect to wavelength, as shown in Fig. 5*a*. This feature results from the relation $\Delta T = T(\lambda_0 + \Delta\lambda) - T(\lambda_0)$ where λ_0 is the wavelength of the mode and $\Delta\lambda$ is the mode shift. Figure 5*b* shows the probe amplification after correction for the effects of the cavity length modulation. Note the high values at $t = 0$ (>25%) that result from the enhancement of the stimulated emission by the cavity (regenerative amplification). Also seen in this figure is the dynamic shift of the mode peak, with significant positive gain present until 64 ps. The results shown in Fig. 5 are fully consistent with the demonstration of lasing, shown earlier, and taken together these provide very direct support for the model in which the main photoexcitation in high-quality PPV is the intrachain exciton[10].

We have demonstrated lasing in a high-Q microcavity device based on PPV. This has the structure appropriate for electrical pumping (in contrast to structures which use conjugated polymers in solid or liquid solutions[21,22]), although much remains to be done to improve the ease with which charge can be injected into the PPV. We conclude nevertheless that the quality of present polymers has reached a point where they can be considered as electrically pumped lasers for highly demanding device applications. □

Received 19 June; accepted 15 July 1996.

1. Burroughes, J. H. *et al. Nature* **347,** 539–541 (1990).
2. Burn, P. L. *et al. Nature* **356,** 47–49 (1992).
3. Gustafsson, G. *et al. Nature* **357,** 477–479 (1992).
4. Greenham, N. C., Moratti, S. C., Bradley, D. D. C., Friend, R. H. & Holmes, A. B. *Nature* **365,** 628–630 (1993).
5. Berggren, M. *et al. Nature* **372,** 444–446 (1994).
6. Greenham, N. C. & Friend, R. H. in *Solid State Physics* **49** (eds Ehrenreich, H. & Spaepen, F. A.) 2–150 (Academic, San Diego, 1995).
7. Yan, M., Rothberg, L., Hsieh, B. R. & Alfano, R. R. *Phys. Rev. B* **49,** 9419–9422 (1994).
8. Yan, M., Rothberg, L. J., Papadimitrakopolous, F., Galvin, M. E. & Miller, T. M. *Phys. Rev. Lett.* **72,** 1104–1107 (1994).
9. Yan, M., Rothberg, L. J., Kwock, E. W. & Miller, T. M. *Phys. Rev. Lett.* **75,** 1992–1995 (1995).
10. Harrison, N. T., Hayes, G. R., Phillips, R. T. & Friend, R. H. *Phys. Rev. Lett.* (in the press).
11. Yamamoto, Y., Machida, S. & Björk, G. *Opt. Quantum Electronics* **24,** S215–S243 (1992).
12. Dodabalapur, A., Rothberg, L. J., Miller, T. M. & Kwock, E. W. *Appl. Phys. Lett.* **64,** 2486–2488 (1994).
13. Tsutsui, T., Takada, N., Saito, S. & Ogino, E. *Appl. Phys. Lett.* **65,** 1868–1870 (1994).
14. Lemmer, U. *et al. Appl. Phys. Lett.* **66,** 1301–1303 (1995).
15. Wittmann, H. F. *et al. Adv. Mater.* **7,** 541–544 (1995).
16. Fisher, T. A. *et al. Appl. Phys. Lett.* **67,** 1355–1357 (1995).
17. Grüner, J., Cacialli, F. & Friend, R. H. *J. Appl. Phys.* **80,** 207–215 (1996).
18. Greenham, N. C. *et al. Chem. Phys. Lett.* **241,** 89–96 (1995).
19. Hsu, J. W. P., Yan, M., Jedju, T. M., Rothberg, L. J. & Hsieh, B. R. *Phys. Rev. B* **49,** 712–715 (1994).
20. Harvey, E. J. thesis, Univ. Cambridge (1995).
21. Moses, D. *Appl. Phys. Lett.* **60,** 3215–3216 (1992).
22. Hide, F., Schwartz, B. J., Diaz-Garcia, M. A. & Heeger, A. J. *Chem. Phys. Lett.* **256,** 424–430 (1996).

ACKNOWLEDGEMENTS. We thank Cambridge Device Technology (CDT) for supplying the PPV precursor used in our research. This work is supported by the Engineering and Physical Sciences Research Council and by the Commission of the European Community, ESPRIT Basic Research Programme. It is also part of a collaborative programme with the Chemistry group of A. B. Holmes and S. C. Moratti in Cambridge.

CORRESPONDENCE should be addressed to R.H.F. (e-mail: rhf10@cam.ac.uk).

A chemical-detecting system based on a cross-reactive optical sensor array

Todd A. Dickinson*, Joel White†, John S. Kauer† & David R. Walt*

* The Max Tishler Laboratory for Organic Chemistry, Department of Chemistry, Tufts University, Medford, Massachusetts 02155, USA
† The Department of Neuroscience, Tufts School of Medicine, Boston, Massachusetts 02111, USA

THE vertebrate olfactory system has long been recognized for its extraordinary sensitivity and selectivity for odours. Chemical sensors have been developed recently that are based on analogous distributed sensing properties[1–4], but although an association between artificial devices and the olfactory system has been made explicit in some previous studies[4,5], none has incorporated comparable mechanisms into the mode of detection. Here we describe a multi-analyte fibre-optic sensor modelled directly on the olfactory system, in the sense that complex, time-dependent signals from an array of sensors provide a 'signature' of each analyte. In our system, polymer-immobilized dye molecules on the fibre tips give different fluorescent response patterns (including spectral shifts, intensity changes, spectral shape variations[6] and temporal responses) on exposure to organic vapours, depending on the physical and chemical nature (for example, polarity, shape and size) of both the vapour and the polymer. We use video images of temporal responses of the multi-fibre tip as the input signals to train a neural network for vapour recognition. The system is able to identify individual vapours at different concentrations with great accuracy. 'Artificial noses' such as this should have wide potential application, most notably in environmental and medical monitoring.

A critical problem solved by the sense of smell is how to incorporate into a single system both selectivity for many disparate chemicals (broad-band response) and high sensitivity. One way to achieve this would be to have a multitude of specific receptors with high binding coefficients, one for each molecule of interest to the organism. There is little experimental evidence for this, with the exception of pheromone detection in insects where a specific ligand/receptor/neural pathway seems to exist[31]. In vertebrates, however, physiological, anatomical, biochemical and lesion studies all support the view that the distinctive molecular signatures of odour compounds are encoded by cross-reactive receptor cells, in conjunction with neuronal integrative circuits, by the generation of response patterns that are widely distributed in space and time[7]. Using similar spatio-temporal patterning, we have incorporated a number of these biological properties into an odour sensing device. As in previously developed systems[2,4,8–13], this device does not rely on specifically selective sensors. The crucial element of such systems is to capture information about the analyte molecule in a distributed fashion that is encoded sufficiently to allow discrimination from other closely related chemical structures.

In an effort to implement this concept of distributed detection, we have incorporated an array format into the construction of the sensor, using a bundle of 19 individual multi-mode optical fibres. In recent years, the array approach has also been taken by others in the development of vapour sensors based on surface-acoustic-wave (SAW)[2,8,9], electrochemical[10], conducting polymer[4,11] and piezoelectric[12,13] methods. Conductive polypyrroles, for example, are now being used in commercial devices to identify odours based on the conductivity changes that occur as analytes adsorb onto the sensor surface. Acoustic-wave-based sensors, on the other hand, measure frequency deviations associated with the slight mass changes induced by vapour molecules adsorbing onto oscillating, polymer-coated quartz sensors. Because each of the current